Giftet Inc.
Journal of Geolocation, Geo-information, and Geo-intelligence
Volume 2023, article ID 2023071601, 18 pages
http://doi.org/10.18610/JG3.2023.071601

Research Article

Discrete vs. Continuous Carrier Tracking Loop with Large BnT: Part 1, Theory[i]

Ilir F. Progri[1], Clifford W. Kelley[2], Guojiang Gao[3], William R. Michalson[4], Jinling Wang[5], and John Lavrakas[6]

[1] *Giftet Inc., 5 Euclid Ave. #3, Worcester, MA 01610, USA*
[2] *Open Source GPS, CA, USA*
[3] *University of Calgary, Canada*
[4] *Electrical and Computer Engineering Department, Worcester Polytechnic Institute, Worcester, MA 01609, USA*
[5] *University of New South Wales, Sydney, Australia*
[6] *Advanced Research Corp., Newport, OR*
ORCID: 0000-0001-5197-1278

Correspondence should be addressed to Ilir Progri; iprogri@giftet.com.

Received June 7, 2023; Revised June 8, 2023-July 10, 2023, Accepted July 16, 2023; Published November 1, 2023.

Editor-in-Chief/ Senior Scientific Editor: Ilir F. Progri

Abstract—The majority of textbooks (e.g., Kaplan, Hegarty 1996) appear to provide an analog or continuous representation on the theory of carrier tracking loops based on continuous tracking loop equations. Such a representation may be adequate to explain the tracking loop phenomenon when the *noise bandwidth* (B_n) *integration time* (T) product is much less than *one* where we are able to predict and explain the observed input/output relationship based on continuous carrier tracking theory (or equations). But, as soon as this product gets large than *one* then there appears to be an inconsistency between observed results and those predicted from the continuous tracking loops (Stephens, Thomas 1995). To investigate this inconsistency and be able to explain the lack of consistency between the published theory and experimental data we implemented the carrier-tracking loop for Open-Source GPS using the same integration time for the carrier and code loops equal to the twenty-millisecond data period. First, we tracked in accumulated carrier phase by setting the loop bandwidth approximately equal to twenty Hz, which produces a B_nT equal to one half. Initially the carrier tracking loop appeared to work well but, later the position and to a larger extent the velocity fixes accumulated more and more error. Second, since it was known that this loop works well with an integration time of one millisecond it motivated us on to investigate this phenomenon in greater detail.

It is known that, when B_nT is close to or above one, field test results are not consistent with the theoretical expectation (e.g., Kaplan, Hegarty 1996) any more. It is obvious that the theory should be corrected in this case to reflect our learned knowledge from the observations. In (Gao 2007) it is given an understanding on this issue and an explanation for signal tracking errors of both Frequency Locked Loop (FLL) and Phase Locked Loop (PLL) in a digital GNSS receiver. Based on the knowledge derived from these formulae, even when the receiver clock noise and the signal-Doppler tracking error are constant, they generate larger and larger signal tracking errors when B_nT increases. However, this phenomenon is not observed in the classic GPS tracking theory. It was suggested that this could be symptomatic (or indicative or characteristic) of a carrier-tracking loop with a large B_nT. This effect is a part of G. Gao's Ph.D. research in which he has come up with a suggested solution to this phenomenon (Gao, 2007). Furthermore, in this paper, Dr. Progri provided a revised, complete derivation of the stability condition of the discrete-time tracking loop based on the condition of the stability of the system function and also of the discrete-time unit pulse function.

In part one of this journal paper, we performed the analysis of this phenomenon and then in part two of another journal paper (see Progri et al. 2023) we verified it with data from tests with the Open-Source GPS software receiver emulation (theoretical or ideal signal) and then with the GP2015/2021 hardware (with a real GPS signal coming from a GPS satellite). The results presented include our theoretical approach and the experimental data (see Progri et al. 2023). According to our analysis it appears that for $0 < B_nT < 0.3329$ the carrier tracking is stable; however, for $0.3329 < B_nT \leq 0.5$ the carrier tracking is marginally stable; i.e., it stable in short term or for a few seconds and unstable in the long term or for many seconds, minutes, hours etc. The results of the implementation and test are presented in the part two in another paper (see Progri et al. 2023)).

Index Terms—Carrier tracking, integration time, loop bandwidth, TCXO, Open-Source GPS.

1 Introduction

An optimal estimator-based GPS receiver aims at obtaining more signal tracking processing gain than regular technologies. The first approach of the deeply integrated GPS-based navigator is the Vector Delay Locked Loop (DLL) or (VDLL) technique proposed by Parkinson, Spilker (1996, [2]). Zhodzishsky, Yudanov (1998, [3]), introduced a COOP tracking architecture design, which fuses information from the tracking channels to track (estimate) code phase, carrier phase, Doppler shift, rate of change of Doppler shift, carrier amplitude and data bit sign, with variances of the estimate states. Gustafson, Dowdle (2000, [4]), on the other hand, utilized optimal estimation techniques to track (estimate) code phase, carrier phase, Doppler shift, rate of change of Doppler shift, carrier amplitude and data bit sign by fusing all channel measurements. This entire optimal estimation-based receiver is called deeply integrated GPS-based navigator with optimal estimators (Zhodzishsky, Yudanov (1998, [3]), Gustafson, Dowdle (2000, [4]), Psiaki, Jung (2002, [5])).

From 1996 until 2002, GPS receiver augmentation technologies, the integrated optimal estimators bring very significant processing gain to the GPS signal tracking loops and make possible the tracking on GPS carrier phase under attenuated signal environments (Gustafson, Dowdle (2000, [4]), Psiaki, Jung (2002, [5])).

For decades, GPS receivers have been designed and developed employing classical control theory, which is consistent with modern digital communication theory. Optimal estimator-based GPS receiver enhancements; however, improved receiver performance based on modern control theory can result is a significant enhancement in GPS receiver design. Nevertheless, the optimal estimator-based method still cannot meet the requirements for urban canyon and indoor navigation completely Progri, (2003, [6]), Progri et al (2007, [7]), Progri et al (2016, [8]) Progri, Michalson (2020, [9]). Table I shows its characteristics under attenuated signals.

The majority of textbooks (e.g., Kaplan, Hegarty (1996, [10])) appear to provide an analog or continuous representation on the theory of carrier tracking loops based on continuous tracking loop equations. Such a representation may be adequate to explain the tracking loop phenomenon when the *noise bandwidth* (B_n) *integration time* (T) product is much less than *one* where we are able to predict and explain the observed input/output relationship based on continuous carrier tracking theory (or equations). But, as soon as this product gets large than one then there appears to be an inconsistency between observed results and those predicted from the continuous tracking loops (Stephens, Thomas (1995, [15])). In order to investigate this inconsistency and be able to explain the lack of consistency between the published theory and experimental data we implemented the carrier-tracking loop for Open-Source GPS using the same integration time for the carrier and code loops equal to the 20 ms data period. First, we tracked in accumulated carrier phase by setting the loop bandwidth approximately equal to 25 Hz, which produces a B_nT of 0.5. Initially, the carrier tracking loop appeared to work well but, later on the position and to a larger extent the velocity fixes accumulated more and more error. Second, since it was known that this loop works well with an integration time of 1ms it motivated (or gave us the incentive) us on to look into this phenomenon in greater detail.

It is known that, when B_nT is close to or above one, field test results were not consistent with the theoretical expectation (e.g., Kaplan, Hegarty (1996, [10]) any more. It is obvious that the theory should be corrected in this case to reflect our learned knowledge from the observations. In (Gao (2007, [16])) it is given an understanding on this issue and an explanation for signal tracking errors of both FLL and PLL in a digital GNSS receiver. From the knowledge derived from these new formulae, one can infer that, even when the receiver clock noise and the signal-Doppler tracking error are constant, they generate larger and larger signal tracking errors when B_nT increases. However, this phenomenon is not observed in the classic GPS tracking theory. It was suggested that this could be symptomatic (or indicative or characteristic) of a carrier-tracking loop with a large B_nT. This effect was a part of G. Gao's Ph.D. research in which he came up with a suggested solution to this phenomenon (Gao (2007, [16])). Furthermore, in this paper, Dr. Progri provided a revised, complete derivation of the stability condition of the discrete-time tracking loop based on the system function and the unit pulse function.

We first performed the analysis of this phenomenon and then in Progri et al (2023, [23]) we verified it with data from tests with the Open-Source GPS software receiver emulation (theoretical or ideal signal) and then with the GP2015/2021 hardware (with a real GPS signal coming from a GPS satellite). The results presented include our theoretical approach in this journal paper and the experimental data in Progri et al (2023, [23]. According to our analysis it appears that for $0 < B_nT < 0.3329$ the carrier tracking is stable; however, for $0.3329 < B_nT \leq 0.5$ the carrier tracking is marginally stable; i.e., it stable in short term or for a few seconds and unstable in the long term or for many seconds, minutes, hours etc.

The paper is organized in the following manner. First, we introduce and discuss (or give an overview of) a classic GPS receiver and emphasize the classic GPS L1 receiver tracking strategy, the features of correlated GPS signals, the design of GPS receiver code DLL, the design of GPS receiver Phase Locked Loop (PLL) and conclude the section with a discussion on PLL/Frequency Locked Loop (FLL) tracking errors for digital GPS receivers. Second, we discuss the GP2021 tracking loops theory and practice with focus on GP2021 channel baseband signal processing, GP2021 discrete-time carrier and code tracking loop theory and practice, and conclude the section with GP2021 discrete-time carrier and code tracking loop implementation. Third, we present a summary and conclusion section. Fourth, we provide a future work section. Appendix A contains the revised inequality of the B_nT that is used to explain the inconsistency that existed between the theory and practice of digital GPS receivers.

2 An Overview of a Classic GPS Receiver

Section 2 contains three subsections: (1) classic GPS L1 receiver tracking strategy; (2) features of correlated GPS signals; (3) design of classic GPS receiver code DLL.

2.1 Classic GPS L1 receiver tracking strategy

After the signals broadcasted by satellite arrive at the receiver's antenna(e), the signal propagating through the radio frequency (RF) band is first down-converted to the intermediate frequency (IF) band in the RF module of the receiver, and then signal acquisition is performed by the receiver baseband processor and simultaneously performing the Doppler and code removal. After signal down conversation and acquisition, the GPS IF signal is transmitted into the signal tracking loops for code delay and carrier phase coherent tracking to recover the incoming signal accurately (Kaplan, Hegarty (1996, [10])). GPS signal tracking loops contain the code DLL and carrier PLL. Figure 1 shows the architecture of the GPS baseband signal tracking loops. These two loops normally work in parallel: The DLL replicates the incoming code to cancel the effect of the Pseudo-Random-Noise (PRN) code; and simultaneously, the PLL replicates the incoming carrier phase and remove the carrier from the incoming signal.

Because of the navigation data bits modulated on GPS signal, the PLL usually uses a Costas loop, which is insensitive to 180° data bit reversal (Kaplan, Hegarty (1996, [10])). The disadvantage of using the Costas tracking loop is that there is a 6 dB tracking-sensitivity loss as compared to a Pull-PLL (P-PLL) (e.g., Julien (2005, [11], [12])).

TABLE I: THE CHARACTERISTICS OF OPTIMAL ESTIMATOR TRACKING METHOD UNDER ATTENUATED SIGNALS

Items	*Rating*	*Description (Zhodzishsky et al. (1998, [3]); Gustafson et al. (2000, [4]))*
Tracking Sensitivity	Fair	15-25 dB additional Gain (compared to standard GPS receivers), not enough for fading GPS signal positioning.
Acquisition Sensitivity	Good	Information obtained from acquired signals may be used to speed acquisition processing of the other signals, especially in hot starts.
Re-acquisition Ability	Good	Re-acquisition of unlock channels will be aided by other locked channels.
Data Output Rate	Fair	The Kalman filter in tracking loops cannot be performed with a high recursive rate.
Positioning Accuracy	Good	The best performance can be achieved in fading signal environments for its optimal nature.
Carrier phase output	Good	By enhancing PLLs, this method can output phase observations and reduce/avoid cycle slips.
Dynamic response	Fair	It can meet the requirements for most commercial low-dynamics applications.
Receiver Size	Small	No need for any other hardware. Can be realized in GPS receiver software.
Power Cost	Low	No other hardware required, so no additional power cost.
Anti-multipath Ability	Bad	Channels affect each other when fused, multipath signals in environments pollute the filter estimation and, thus, degrade this technology. *

(*: If a strong echo-only signal is received by a standard receiver, the latter still works but with a poor positioning accuracy. For a receiver with an optimal estimator, however, it might lose lock on all channels because of the echo-only signal, and, thus, does not work at all.)

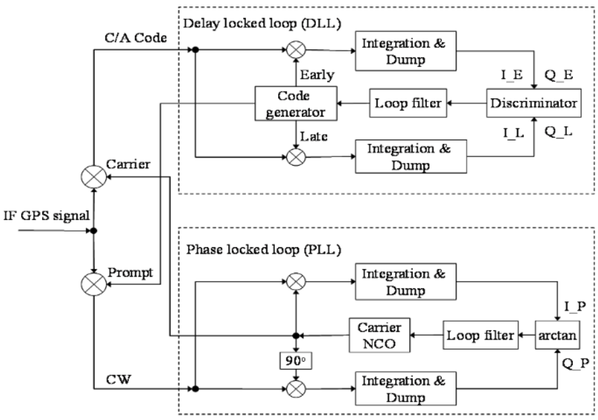

FIGURE 1: Architecture of GPS signal tracking loops.

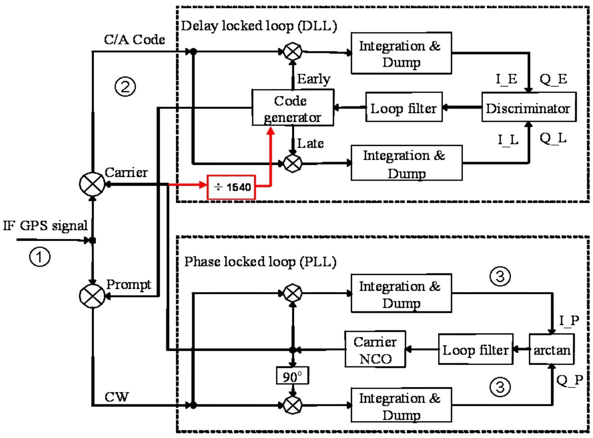

FIGURE 2: Architecture of PLL-assisted DLL.

For this reason, the PLL is more sensitive to environment noise, interference, and jamming, as compared to DLL (Progri Chap. 6 (2011, [13])). In GPS signal tracking, it is usually the PLL that first loses lock, and then the DLL loses lock since the receiver cannot correctly replicate the incoming signal carrier phase (Kaplan, Hegarty (1996, [10])).

Since the C/A code is modulated on the carrier wave, the code Doppler can be computed using the carrier Doppler as:

$$f_{Dc} = \frac{f_c}{f_C} \times f_{DC} = 1540 \times f_{DC} \qquad (1)$$

To improve the accuracy of the DLL, a PLL-assisted DLL architecture is regularly used in GPS signal tracking, as shown in Fig. 2. Based on (1), the carrier Doppler from the PLL is divided by a factor of 1540 and then fed into the code generator for code tracking (Kaplan, Hegarty (1996, [10])).

Since external aiding from the carrier loop is applied to compensate for most of code tracking errors and therefore improve DLL tracking performance, DLLs here only need to correct some insignificant errors, such as initial tracking errors, the rate of change of the ionosphere or differences in code and multipath. These residual variations are normally small and change very slowly with time in open-sky environments. Thus, the DLL loop bandwidth can be significantly reduced to an order of 0.05 to 1 Hz, depending on the application. With external aiding from the carrier loop, the pre-detection time can be extended dramatically based on the Doppler aiding accuracy (Kaplan, Hegarty (1996, [10])). In personal/vehicle navigation applications in weak signal environments, the multipath error might be very large and change very quickly Progri (2021, [14]). Fortunately, with Inertial Navigation System (INS) aiding, it is possible for the INS-assisted GPS receiver to track on Line-Of-

Sight (LOS) signal directly and avoid tracking the rapidly changed multipath signals.

Carrier tracking loops can be divided into two classes: PLLs to track the incoming carrier phase and Frequency Locked Loops (FLL) to track the incoming carrier frequency. Now a GPS receiver usually uses a FLL-assisted PLL for carrier tracking. FLL generates the uncorrelated local carrier wave whose frequency is the same as the incoming signal, but whose phase can be different from the phase of the incoming signal, while PLL generates the correlated local carrier wave whose frequency and phase are both the same as the incoming signal. Compared to a FLL, a PLL provides more accurate carrier phase measurements but tends to lose track under adverse situations. The FLL-assisted PLL design takes advantage of the robustness of FLL and the accuracy of PLL (Kaplan, Hegarty (1996, [10])).

2.2 Features of correlated GPS signals

The incoming GPS signal can be expressed as follows Raquet (2004, [17]):

$$r(t) = A \cdot D \cdot \mathrm{CA}(\beta t - \tau) \cdot \cos(\phi_c)$$
$$= a(t,\tau) \cdot \cos(\phi_c) \quad (2)$$
$$\beta = 1 + f_D / f_c \quad (3)$$
$$\phi_c = (\omega_c + \omega_D)t + \phi_0 \quad (4)$$

where A is the signal amplitude, D is navigation data bit, CA is the C/A pseudo-random code, f_D is the code Doppler and f_c is the C/A chip rate on L_1 frequency. τ is the code delay which is the distance from the satellite to the receiver in units of time, e.g., seconds. ω_c and ω_D are carrier frequency and carrier Doppler.

After the frequency down conversion and carrier phase wiping off (or canceling), the output signals shown in Fig. 2 are as follows Raquet (2004, [17]):

$$I_2 = I_1 \cos(\omega_r t) + Q_1 \sin(\omega_r t) \quad (5)$$
$$Q_2 = Q_1 \cos(\omega_r t) - I_1 \sin(\omega_r t) \quad (6)$$

where ω_{IF} is the intermediate frequency which is down-converted from the L1 frequency, ω_{ref} is the frequency of local replica, ϕ_0 represents the initial carrier phase and

$$I_1 = a_1(t,\tau)c_1 \quad (7)$$
$$Q_1 = a_1(t,\tau)s_1 \quad (8)$$
$$a_1(t,\tau) = a(t,\tau)/\sqrt{2} \quad (9)$$
$$\phi_1 = (\omega_{\mathrm{IF}} + \omega_D)t + \phi_0 \quad (10)$$
$$c_1 = \cos(\phi_1) \quad (11)$$
$$s_1 = \sin(\phi_1) \quad (12)$$

Substituting (7) and (8) into (5) and (6) yields:

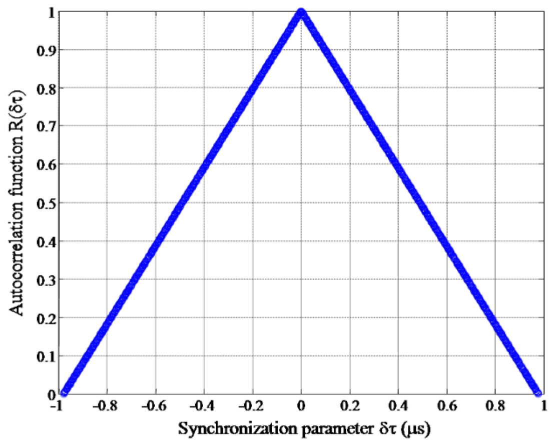

FIGURE 3: PRN code autocorrelation function.

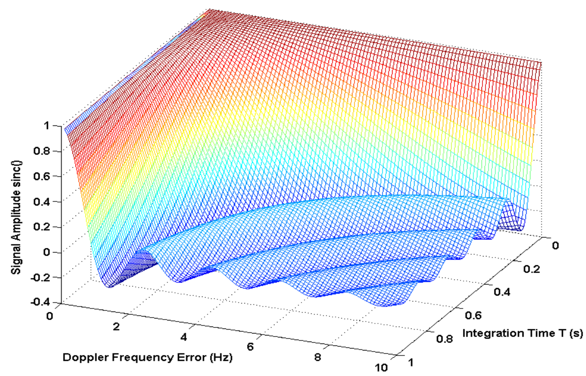

FIGURE 4: Signal amplitude attenuation over Doppler frequency error and integration time; I.

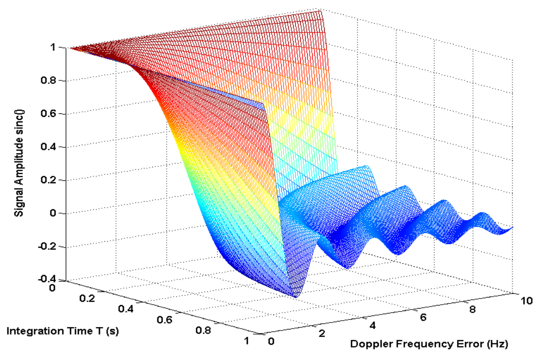

FIGURE 5: Signal amplitude attenuation over Doppler frequency error and integration time; II.

$$I_2 = a_1(t,\tau)c_2 \quad (13)$$ [ii]
$$Q_2 = a_1(t,\tau)s_2 \quad (14)$$ [iii]
$$\phi_2 = (\omega_{\mathrm{IF}} + \omega_D - \omega_r)t + \phi_0 \quad (15)$$

In some commercial GPS receivers, there is only one in-phase I_1 component output from the front end and the quadra-phase Q_1 component is not available. Equations (13) and (14) then become:

$$I_2 = I_1\cos(\omega_r t) \cong a_2(t,\tau)c_2 \quad (16)$$

$$Q_2 = -I_1\sin(\omega_r t) \cong a_2(t,\tau)s_2 \quad (17)$$

$$a_2(t,\tau) = a_1(t,\tau)/2 \quad (18)$$

(after low pass filter)

In (17), it is clear that the quadra-phase Q_2 component is the negative of the product of the incoming signal I_1 and the local carrier.

After a low pass filter, (13)/(14) and (16)/(17) are almost the same, except for a factor of 0.5 in (16)/(17). Equation (13)/(14), which is for the more general case, will be used for future analysis.

In Fig. 2, after signal correlation and dumping, one can write Raquet (2004, [17])

$$I_3 = a_3(t,\delta\tau)c_3{}^{\mathrm{iv}} \quad (19)$$

$$Q_3 = a_3(t,\delta\tau)s_3{}^{\mathrm{v}} \quad (20)$$

$$a_3(t,\delta\tau) = A_d \cdot R(\delta\tau) \quad (21)$$

$$A_d = \left(A/\sqrt{2}\right)\cdot M_{\mathrm{E}}\cdot D\cdot[\mathrm{sinc}(\Delta\varphi) \equiv \sin(\Delta\varphi)/\Delta\varphi] \quad (22)$$

$$\phi_3 = \Delta\varphi + \phi_0 \quad (23)$$

$$\Delta\varphi = \pi\Delta f T \quad (24)$$

where T is the Pre-detection Integration Time (PIT), $\delta\tau$ is the code delay misalignment which depends on range of the Temperature Compensated Cristal Oscillator (TCXO)[vi], M_{E} is the sampling number in T, and $R(\delta\tau)$ is the PRN code autocorrelation function and expressed as (see Fig. 3)

$$R(q) = \begin{vmatrix} 1-\frac{L_{+1}}{LT_c}|q| & \approx 1-\frac{1}{T_c}|q|, & |q \equiv \delta\tau| \le T_c \\ -\frac{1}{L} & \approx 0, & T_c < |q| \le L_{-1}T_c \end{vmatrix} \quad (25)$$

$$L_{\pm 1} = L \pm 1 \quad (26)$$

where L is the chip numbers of the PRN C/A code (1023) and T_c is the PRN code chip interval.

Equation (19)/(20) shows clearly the four main factors which limit the Signal-to-Noise Ratio (SNR):

1. Incoming Signal power A: a weak incoming signal will decrease tracking sensitivity.
2. Navigation data bit D: the unknown nature of navigation data will limit the coherent integration time.
3. Code-delay misalignment $\delta\tau$: A code-delay alignment error will decrease the signal power after de-spreading, with the power loss characterized by the function $R(\delta\tau)$. Figure 3 illustrates the signal degradation due to code-delay misalignment $\delta\tau$.
4. Doppler error Δf: the tracking difference between the local replica carrier frequency whose stability is a function of the TCXO and the incoming carrier frequency will lead to signal power loss when doing coherent integration. The loss is characterized by the function $\mathrm{sinc}(\Delta\varphi)$ whose stability is a function of the TCXO and is illustrated in Figs. 4 and 5.

Figures 4 and 5 show two plots of the signal amplitude attenuation due to Doppler frequency error and integration time. As shown in both figures, to decrease the signal power loss characterized by the function $\mathrm{sinc}(\Delta\varphi)$, both the Doppler frequency error and integration time should keep small. However, from (19)/(20), it is clear that a shorter integration time will lead to a small value of M_{E} and thus decrease the accumulated signal power, which is not desired. Therefore, there is a balance in choosing the integration time for weak signal tracking.

There are several reasons that might lead to the mismatch Δf of the incoming Doppler with the local replica, namely satellite motion, receiver dynamics, TCXO oscillator instability, etc. In previous research (Watson (2005, [18])), the contributions of propagation effects were shown to be negligible for stationary receivers, contributing up to a 0.01 Hz random error, and up to a 0.13 Hz constant bias, although average values are expected to be lower. These random errors are insignificant until reaching or exceeding a full 10 s of coherent integration. In summary, the only significant factors likely to limit coherent integration for stationary receivers are the errors in the receiver oscillator or TCXO for example. If the oscillator or TCXO under test is proved capable of supporting coherent integration of up to 10s, at which point satellite oscillator errors and propagation errors might become factors, this assumption can be re-evaluated. So, in all these factors, receiver dynamics and oscillator or TCXO instability are the two most important error sources.

2.3 Design of classic GPS receiver code DLL

Starting with an introduction of DLL architecture, this section analyzes three commonly used DLL discriminators in terms of their processing gain and normalization effects. The research's emphasis is to find a discriminator capable of achieving the highest discriminator gain and the widest phase error pull-in range in degraded signal environments. Next, effects of loop filters on signal tracking are discussed, with the focus on the analysis of loop characteristics, e.g., tracking error pull-in/pull-out range, loop pull-in time, loop natural frequency and so on.

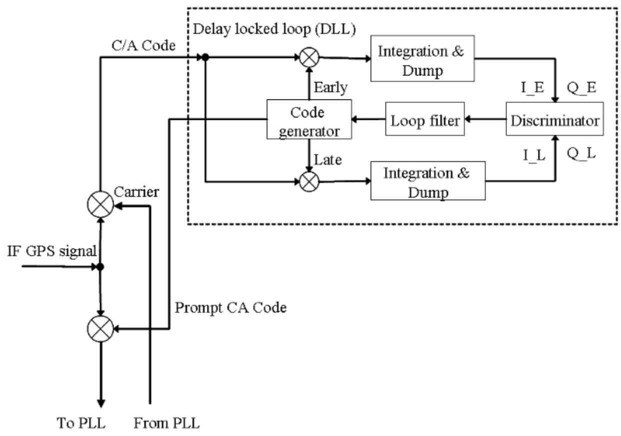

FIGURE 6: An architecture or a carefully designed block diagram of a generic DLL.

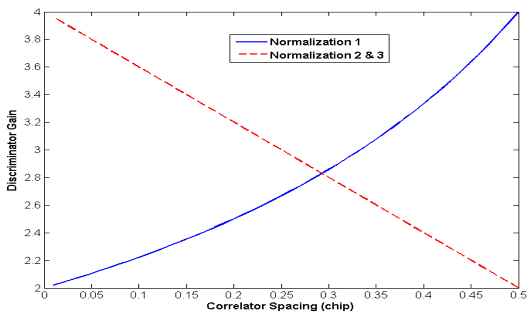

FIGURE 7: Processing gains after discriminator normalization.

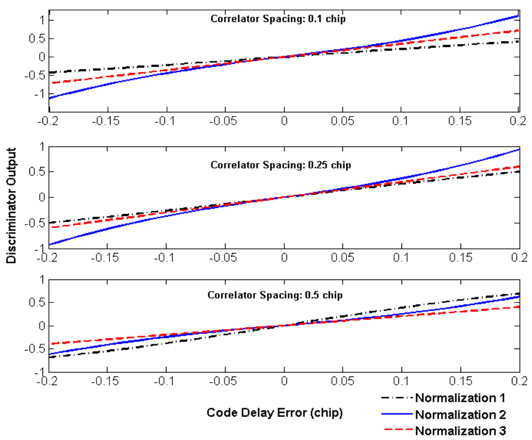

FIGURE 8: Discriminator products after normalization.

Using (17)/(18), I_E, Q_E, I_L, and Q_L in Fig. 6 can be written as follows Raquet (2004, [17]):

$$I_E = a_3(t, \delta\tau - \delta)c_3 \tag{27}$$

$$Q_E = a_3(t, \delta\tau - \delta)s_3 \tag{28}$$

$$I_L = a_3(t, \delta\tau + \delta)c_3 \tag{29}$$

$$Q_L = a_3(t, \delta\tau + \delta)s_3 \tag{30}$$

where δ is correlator spacing.

In order to obtain the best DLL performance under weak signal tracking, the discriminator and its normalization algorithm with the highest processing gain are selected herein. Three well-known DLL discriminators proposed by Kaplan, Hegarty (1996, [10]) are:

$$B_1(\delta\tau) = (I_E - I_L)I_P + (Q_E - Q_L)Q_P \tag{31}$$

$$B_2(\delta\tau) = (I_E^2 + Q_E^2) - (I_L^2 + Q_L^2) \tag{32}$$

$$B_3(\delta\tau) = \sqrt{I_E^2 + Q_E^2} - \sqrt{I_L^2 + Q_L^2} \tag{33}$$

Substituting (27) through (30) into (31) through (33) yields

$$B_1(\delta\tau) = A_d^2[R(\delta\tau - \delta) - R(\delta\tau + \delta)]R(\delta\tau) \tag{34}$$

$$B_2(\delta\tau) = A_d^2[R^2(\delta\tau - \delta) - R^2(\delta\tau + \delta)] \tag{35}$$

$$B_3(\delta\tau) = A_d[R(\delta\tau - \delta) - R(\delta\tau + \delta)] \tag{36}$$

and inserting (25) into (34) through (36), when $|\delta\tau| \le \delta$, yields

$$\begin{aligned} B_1(\delta\tau) &= \frac{A_d^2}{T_c}[|\delta\tau + \delta| - |\delta\tau - \delta|]\left(1 - \frac{1}{T_c}|\delta\tau|\right) \\ &= (A_d^2/T_c^2)2\delta\tau(T_c - |\delta\tau|) \end{aligned} \tag{37}$$

$$\begin{aligned} B_2(\delta\tau) &= A_d^2\left[\left(1 - \frac{1}{T_c}|\delta\tau - \delta|\right)^2 - \left(1 - \frac{1}{T_c}|\delta\tau + \delta|\right)^2\right] \\ &= A_d^2\left|\begin{array}{l} \left(\frac{1}{T_c}\right)^2(\delta - \delta\tau)^2 - \left(\frac{1}{T_c}\right)^2(\delta + \delta\tau)^2 \\ +2\frac{1}{T_c}(\delta + \delta\tau) - 2\frac{1}{T_c}(\delta - \delta\tau) \end{array}\right. \\ &= (A_d^2/T_c^2)4\delta\tau(T_c - \delta) \end{aligned} \tag{38}$$

$$\begin{aligned} B_3(\delta\tau) &= A_d[R(\delta\tau - \delta) - R(\delta\tau + \delta)] \\ &= A_d\left[1 - \frac{1}{T_c}|\delta\tau - \delta| - 1 + \frac{1}{T_c}|\delta\tau + \delta|\right] \\ &= (A_d/T_c)(\delta\tau - \delta + \delta\tau + \delta) \\ &= (A_d/T_c)2\delta\tau \end{aligned} \tag{39}$$

The discriminator gain is defined as the slope of B at $\delta\tau = 0$. Therefore, the processing gains of the three discriminators are defined as the derivatives of (37) through (39):

$$\begin{aligned} B_1'(\delta\tau = 0) &= \frac{d}{d\delta\tau}\left[\frac{A_d^2}{T_c^2}2(T_c \mp \delta\tau) \mp \frac{A_d^2}{T_c^2}2\delta\tau\right] \\ &= 2\,A_d^2/T_c \end{aligned} \tag{40}$$

$$\begin{aligned} B_2'(\delta\tau = 0) &= \frac{d}{d\delta\tau}\left[\frac{A_d^2}{T_c^2}4\delta\tau(T_c - \delta)\right] \\ &= 4(A_d^2/T_c^2)(T_c - \delta) \end{aligned} \tag{41}$$

$$\begin{aligned} B_3'(\delta\tau = 0) &= \frac{d}{d\delta\tau}\left[2\frac{A_d}{T_c}\delta\tau\right] \\ &= 2\,A_d/T_c \end{aligned} \tag{42}$$

Equations (40) through (42) clearly indicate that the discriminator gain of discriminators one and three is independent of the correlator spacing δ. The gain for discriminator two increases when correlator spacing δ decreases. When correlator spacing is $\delta = 0.25$ chip, then we obtain the gain of $B_2(\delta\tau)$ as follows

$$B_2'\left(\delta\tau = 0, \delta = \tfrac{1}{4}T_c\right) = 4\frac{A_d^2}{T_c^2}\left(T_c - \tfrac{1}{4}T_c\right)$$
$$= 3\, A_d^2/T_c \quad (43)$$

When correlator spacing is $\delta = 0.1$chip, then we obtain the gain of $B_2(\delta\tau)$ as follows

$$B_2'\left(\delta\tau = 0, \delta = \tfrac{1}{10}T_c\right) = 4\frac{A_d^2}{T_c^2}\left(T_c - \tfrac{1}{10}T_c\right)$$
$$= (18/5 \equiv 3.6)\, A_d^2/T_c \quad (44)$$

It is suggested that Narrow Correlator™ spacing is preferred in order to reduce multipath and thermal noise; hence, discriminator two is selected to maximize the processing gain.

Signal power in urban canyons or indoor environments might change very quickly due to receiver motion or signal masking due to the presence of buildings Progri (2003, [6])-Progri et al (2020, [9]), Progri (2024, [24]). In order to remove the effect of signal power swing on signal tracking, the GPS signal sign for code tracking in DLL should be normalized. In this research, three normalization algorithms are presented below. Please note, only the discriminator two is analyzed herein:

$$\|\delta\tau_i\| = \mathrm{num}/\mathrm{den}_i;\ \forall i \in \{1,2,3\} \quad (45)$$
$$\mathrm{num} = (I_E^2 + Q_E^2) - (I_L^2 + Q_L^2) \quad (46)$$
$$\mathrm{den}_1 = (I_E^2 + Q_E^2) + (I_L^2 + Q_L^2) \quad (47)$$
$$\mathrm{den}_2 = I_P^2 + Q_P^2 \quad (48)$$
$$\mathrm{den}_3 = \mathrm{SNR}(M_E N_0/T_s) \quad (49)$$

where T_s is the sample period, M_E is the number of samples accumulated during the integration time T and N_0 is the noise power density.

Instead of using $M_E N_0/T_s$ for the normalization method three in (17), one can de-spread the incoming GPS signal with PRN 37 to estimate the noise power; PRN 37 is reserved for ground testing and is not being broadcasted by any GPS satellite. This approach was adopted in the first-generation software GPS receiver GNSS_SoftRx™ developed by (Ma, Lachapelle, Cannon (2004, [19])).

Inserting (19)/(20) and (37) through (39) into (46) through (49) yields

$$\mathrm{num} = a_3^2(t, \delta\tau - \delta) - a_3^2(t, \delta\tau + \delta)$$
$$= A_d^2 \cdot R^2(\delta\tau - \delta) - A_d^2 \cdot R^2(\delta\tau + \delta) \quad (50)$$
$$\mathrm{den}_1 = a_3^2(t, \delta\tau - \delta) + a_3^2(t, \delta\tau + \delta)$$
$$= A_d^2 \cdot R^2(\delta\tau - \delta) + A_d^2 \cdot R^2(\delta\tau + \delta) \quad (51)$$
$$\mathrm{den}_2 = a_3^2(t, \delta\tau) = A_d^2 \cdot R^2(\delta\tau) \quad (52)$$

$$\|\delta\tau_1\| = \frac{R^2(\delta\tau-\delta) - R^2(\delta\tau+\delta)}{R^2(\delta\tau-\delta) + R^2(\delta\tau+\delta)} = \frac{\frac{1}{T_c^2}4\delta\tau(T_c-\delta)}{\left(1-\frac{1}{T_c}|\delta\tau-\delta|\right)^2 + \left(1-\frac{1}{T_c}|\delta\tau+\delta|\right)^2}$$

$$= \frac{\frac{1}{T_c^2}4\delta\tau(T_c-\delta)}{2-\frac{2}{T_c}|\delta\tau-\delta|+\frac{1}{T_c^2}|\delta\tau-\delta|^2-\frac{2}{T_c}|\delta\tau+\delta|+\frac{1}{T_c^2}|\delta\tau+\delta|^2}$$

$$= \frac{2\delta\tau(T_c-\delta)}{T_c^2 - 2T_c\delta + (\delta\tau)^2 + \delta^2} \quad (53)$$

$$\|\delta\tau_2\| = \frac{R^2(\delta\tau-\delta) - R^2(\delta\tau+\delta)}{R^2(\delta\tau)} = \frac{4\delta\tau(T_c-\delta)}{T_c^2 - 2T_c\delta\tau + (\delta\tau)^2} \quad (54)$$

$$\|\delta\tau_3\| = \frac{4\delta\tau(T_c-\delta)}{\mathrm{SNR}(M_E N_0/T_S)} \quad (55)$$

Therefore, the gain of discriminators after normalization is

$$\frac{\partial}{\partial\delta\tau}\|\delta\tau_1\|_{(\delta\tau=0)} = \frac{2(T_c-\delta)\left(T_c^2-2T_c\delta+(\delta\tau)^2+\delta^2\right) - 4(T_c-\delta)(\delta\tau)^2}{\left(T_c^2-2T_c\delta+(\delta\tau)^2+\delta^2\right)^2}$$

$$= \frac{2(T_c-\delta)}{T_c^2 - 2T_c\delta + \delta^2} \quad (56)$$

$$\frac{\partial}{\partial\delta\tau}\|\delta\tau_2\|_{(\delta\tau=0)} = \frac{4(T_c-\delta)\left[T_c^2-2T_c\delta\tau+(\delta\tau)^2\right] - 2\delta\tau(T_c-\delta)(\delta\tau-T_c)}{\left[T_c^2-2T_c\delta\tau+(\delta\tau)^2\right]^2}$$

$$= \frac{4(T_c-\delta)}{T_c^2} \quad (57)$$

$$\frac{\partial}{\partial\delta\tau}\|\delta\tau_3\|_{(\delta\tau=0)} = \frac{4(T_c-\delta)}{\mathrm{SNR}(M_E N_0/T_S)} \quad (58)$$

Figure 7 shows the processing gains after discriminator normalization. From this figure, it is clear that the processing gain of normalized discriminators two and three increases when correlator spacing δ decreases. The processing gain of normalized discriminator one, however, decreases when the correlator spacing δ decreases.

Figure 8 shows the normalized discriminator output as a function of the code delay error. In Fig. 8, 0.1/0.25/0.5 chips of correlator spacing are used, respectively. It is clear that, when the correlator spacing is 0.1 or 0.25 chip, the normalization method two yields the best discriminator performance. When the correlator spacing is 0.5 chip, the normalization method two is somewhat worse than method one. From Fig. 7, however, it is known that the use of normalization method one will yield a smaller discriminator gain if a narrower correlator spacing is used. So, it is clear that normalization method two provides the best performance if a narrow correlator spacing is required.

In conclusion, it is suggested to use a normalized Early-Minus-Late discriminator for code tracking.

The track arm of the correlator can be set one half chip (or less) early of the late arm. The normalized discriminator is given by

$$\|\delta\tau_2\| = \mathrm{num}/\mathrm{den}_2 \quad (59)$$

TABLE II: CHARACTERISTICS OF DIFFERENT LOOP FILTERS

Loop Order	*Noise Bandwidth*	*Typical Filter Values*	*Steady-State Error*
1	$\omega_n/4$	$B_n = \omega_n/4$	$R_e = \frac{dR}{dt}\frac{1}{\omega_n}$
2	$\omega_n(1+\alpha_2^2)/(4\alpha_2)$	$\alpha_2 = 1.414$ $B_n = 0.53\omega_n$	$R_e = \frac{d^2R}{dt^2}\frac{1}{\omega_n^2}$
3	$\omega_n(\alpha_3 b_3^2 + \alpha_3^2 - b_3)/[4(\alpha_3 b_3 - 1)]$	$\alpha_3 = 1.1, b_3 = 1.1$ $B_n = 0.784\omega_n$	$R_e = \frac{d^3R}{dt^3}\frac{1}{\omega_n^3}$

TABLE III: $C/N_0 = 15$ DB-HZ, EARLY/LATE DISCRIMINATOR

Group No.	*Noise Bandwidth (Hz)*	*Correlator Spacing (chip)*	*Pre-detection Integration Time (s)*	*Tracking Threshold (chip)*	*Thermal Noise (chip)*
1	1	0.5	0.02	0.167	0.715
2	0.5	0.5	0.02	0.167	0.506
3	0.1	0.5	0.02	0.167	0.226
4	0.1	0.2	0.02	0.067	0.067
5	0.1	0.1	0.02	0.033	0.029
6	0.1	0.1	0.1	0.033	0.024
7	0.1	0.1	1	0.033	0.022
8	0.1	0.1	0.1	0.033	0.024
9	0.05	0.1	0.1	0.033	0.017

i.e., when the loop is locked, the track arm will be nominally one quarter chip (or less) early and the late arm one quarter chip (or less) late of the actual.

Gao (2007, [16]) derives the closed-loop transfer function for signal tracking loop systems and illustrates the relationship between the loop characteristics and loop filter parameters. Table II summarizes the characteristics of different loop filters suitable for a GPS receiver (Gao (2007, [16])).

In order to design a stable control system with wider pull-in/pull-out ranges and a shorter pull-in time, a higher loop natural frequency ω_n is preferred.

It is the same with a first-order or third-order system. However, Tab. II shows that the same natural frequency ω_n will lead to different noise bandwidth B_n due to the difference order system as explained further. When the natural frequency ω_n is the same, a first-order system will yield the narrowest noise bandwidth and a third-order system will yield the widest noise bandwidth. It is well known that the narrower the noise bandwidth a DLL adopts, the less thermal noise the receiver will output.

So, in loop filter design, although a higher order system normally provides better steady-state error performance, as shown in Tab. II, a lower order system usually provides shorter response time, better system stability and less thermal noise.

DLL tracking error sources consist mostly of thermal noise, multipath and receiver dynamics (Kaplan, Hegarty (1996, [10])). In order to suppress the DLL tracking error caused by multipath, a narrow correlator technology can be used to minimize this kind of error by reducing the correlator spacing, which, when multiplied by the reflected signal coefficient, bounds the maximum multipath envelope (e.g., Raquet (2004, [17])). As for the receiver dynamic stress error, because the PLL-aided DLL design efficiently decreases the dynamic of DLL to as small as less than 0.1 Hz, the dynamic stress error can be ignored (Kaplan, Hegarty (1996, [10])).

The last and most important portion of DLL tracking error caused by thermal noise is (Kaplan, Hegarty (1996, [10]))

$$\sigma_{DLL,t} = \sqrt{\frac{2\delta^2 B_n}{C/N_0}\left[2(1-\delta) + \frac{4F\delta}{T\cdot C/N_0}\right]} \tag{60}$$

where δ is the correlator spacing between early and prompt or prompt and late, B_n is the noise bandwidth, C/N_0 is the carrier-to-noise ratio in unit of Hz, and T is the PIT. F is a DLL discriminator factor and has a value of 1 for an early/late discriminator or a value of 0.5 for a dot discriminator. With (60), Tab. III lists the tracking errors with nine combinations of different parameter combinations when the C/N_0 is 15 Hz. Please note that, the thermal noise listed in Tab. III is theoretical value. In real applications, the thermal noise will be a little bit larger, since the low pass filter in tracking loops cannot be designed perfectly.

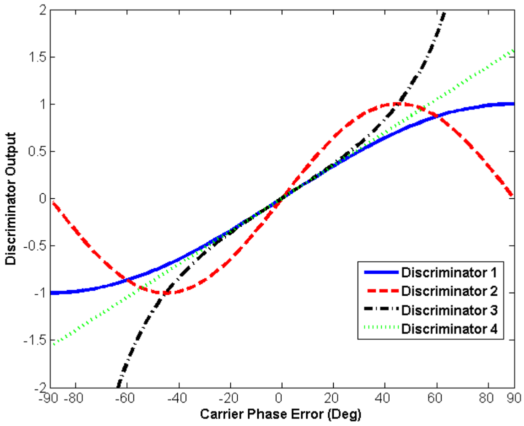

FIGURE 9: Discriminator corrections with respect to carrier phase error.

TABLE IV: PLL DYNAMIC STRESS ERROR

Loop order	*Steady-state error*
1	$R_e = \frac{dR}{dt}\frac{1}{\omega_n} = \frac{1}{4}\frac{dR}{dt}\frac{1}{B_n}$
2	$R_e = \frac{d^2R}{dt^2}\frac{1}{\omega_n^2} = 0.2809\frac{d^2R}{dt^2}\frac{1}{B_n^2}$
3	$R_e = \frac{d^3R}{dt^3}\frac{1}{\omega_n^3} = 0.4828\frac{d^3R}{dt^3}\frac{1}{B_n^3}$

The first three combinations use the same correlator spacing and PIT. The difference is that different noise bandwidths are used to study the effect of noise bandwidth on the DLL tracking error. In combination three, four and five, the correlator spacing parameter is tested for the same purpose. Combinations five, six and seven are used to investigate the PIT. From the results of combinations one to three, one can see that decreasing the noise bandwidth can significantly decrease the DLL thermal noise error.

Decreasing correlator spacing, as shown in combination three to five, can also decrease the thermal noise error. It can however decrease the DLL tracking threshold simultaneously. Combinations four and five show that the DLL tracking capability is only improved marginally when the correlator spacing is decreased from 0.2 chips to 0.1 chips. Increasing PIT in combination five to seven can also decrease thermal noise. When the integration time is above 0.1 s, however, the improvement is very limited.

From the above analysis, the following strategies can be used in order to choose the proper DLL parameters:

1. A noise bandwidth must be as narrow as possible
2. A moderate PIT must coincide with the narrow noise bandwidth
3. A narrow correlator spacing must be used in order to enhance tracking performance in multipath environments

In Tab. III, combinations eight and nine show the two sets of proper DLL parameters for weak signal tracking that are used in this research.

2.4 Classic carrier tracking theory: PLL

Depending on different discriminators used in the PLLs, there are two classes of PLLs: pure PLLs and Costas PLLs. Costas PLLs adopt discriminators, which are insensitive to 180° bit reversals. Costas PLLs, however, suffer 6-dB tracking-sensitivity loss when compared to pure PLLs (Kaplan, Hegarty (1996, [10])). If there were no 50-Hz navigation data modulated on the signal, a pure PLL would be more effective than Costas PLLs in terms of processing gain. Thus, pure PLLs will be used with the GPS L_5 and Galileo frequencies, thanks to the presence of dataless pilot signals. The existence of the navigation bits however, makes Costas PLL necessary for L_1 signal tracking.

In this section, four commonly used PLL discriminators are analyzed in terms of their processing gain and normalization effects. Also, PLL thermal noise, oscillator phase noise and dynamic stress errors are analyzed in order to select carefully the best performance set of parameters including correlator spacing, PIT, and filter order.

2.4.1 PLL discriminator and normalization

Based on the result of (19)/(20), which represents the incoming GPS signal after integration and dump we can write four PLL discriminators as follows:

$$D(1) = \mathrm{sign}(I_P)Q_P/\sqrt{I_P^2 + Q_P^2} \quad (61)$$
$$D(2) = 2I_PQ_P/(I_P^2 + Q_P^2) \quad (62)$$
$$D(3) = Q_P/I_P \quad (63)$$
$$D(4) = \mathrm{atan}(Q_P/I_P) \quad (64)$$

Assuming a phase error bound of $-90° \leq \phi_i \leq \pi\Delta f_i T + \phi_0 \leq 90°$, and inserting (19)/(20) into (61) through (64) yields

$$D(1) = \mathrm{sign}(I_P)Q_P/\sqrt{I_P^2 + Q_P^2} = \sin(\phi_i) \quad (65)$$
$$D(2) = 2I_PQ_P/(I_P^2 + Q_P^2) = \sin(2\phi_i) \quad (66)$$
$$D(3) = Q_P/I_P = \tan(\phi_i) \quad (67)$$
$$D(4) = \mathrm{atan}(Q_P/I_P) = \phi_i \quad (68)$$

Their corresponding discriminator gains are

$$D'^{(1)} = \cos(\phi_i)|_{\phi_i=0} = 1 \quad (69)$$
$$D'^{(2)} = 2\cdot\cos(2\phi_i)|_{\phi_i=0} = 2 \quad (70)$$

TABLE V: PLL PHASE TRACKING ERRORS WITH DIFFERENT PARAMETERS

Group No.	*Noise Bandwidth (Hz)*	*Pre-detection integration time (s)*	*Thermal Noise (°)*	*Allan Deviation Oscillator Phase Noise θ_A (°)*	*Accumulated Oscillator Phase Noise θ_T (°)*	*Dynamics Uncertainty (°)*
1	10	0.001	132.1	2.5	0.06	0.18
2	5	0.001	93.4	5.0	0.06	0.18
3	1	0.001	41.8	25.01	0.06	0.18
4	5	0.001	93.4	5.0	0.06	0.18
5	5	0.01	36.7	5.0	0.6	1.8
6	5	0.1	24.6	5.0	5.7	18
7	2	0.25	14.9	12.6	14.3	45.0

$$D'^{(3)} = \frac{\cos^2(\phi_i)+\sin^2(\phi_i)}{\cos^2(\phi_i)}\bigg|_{\phi_i=0} = \frac{1}{\cos^2(\phi_i)}\bigg|_{\phi_i=0} = 1 \quad (71)$$

$$D'(4) = 1 \quad (72)$$

Figure 9 shows the four discriminator products as a function of the carrier phase errors. From Fig. 9, one can see that the two-quadrant arctangent discriminator D(4) has a balanced performance for both high and low SNR situations. Its processing gain is not dependent on its carrier phase error input. The dot product discriminator D(2) shows good performance when the phase error is in the range of $\pm 45°$ The red line in Fig. 9 shows a slope of close to 2 at the center while others are 1. With the phase error increasing, however, the performance of D(2) decreases quickly. For this reason, the tracking threshold of PLL is normally set 45° (or 15° for 1σ).

D(1) and D(2) are normalized discriminators as presented in (65) through (68). When the C/N_0 is very low, the thermal noise will distort the discriminator slope during normalization. When the incoming signal is very weak, the thermal noise included in the signal becomes significant so that the signal power used to perform discriminator normalization changes to

$$P = (I + n_I)^2 + \left(Q + n_Q\right)^2 \approx (I^2 + Q^2) + \left(n_I^2 + n_Q^2\right)$$
$$\neq I^2 + Q^2 \quad (73)$$

where n_I and n_Q are the in-phase (I), and quadra-phase (Q) thermal noise components.

2.4.2 PLL/FLL tracking errors for digital GPS receivers

The total PLL tracking error ϕ_{PLL} in a continuous GPS receiver includes thermal noise, Allan deviation oscillator phase noise and dynamic stress error. The error can be written in (Kaplan, Hegarty (1996, [10])):

$$\phi_{PLL} = \sqrt{\sigma_{PLL,t}^2 + \theta_A^2} + \theta_e/3 \quad (74)$$

In (74), the PLL thermal noise $\sigma_{\mathrm{PLL,t}}$ is

$$\sigma_{\mathrm{PLL,t}} = \frac{360}{2\pi}\sqrt{\frac{\mathrm{B}_n}{C/N_0}\left(1 + \frac{1}{\mathrm{T}C/N_0}\right)}\,(°) \quad (75)$$

where, B_n is the noise bandwidth of the PLL loop filter, C/N_0 is the carrier-to-noise ratio in unit of Hz, and T is the PIT.

Allan deviation oscillator phase noise θ_A is

$$\theta_A = a\frac{\sigma_A(\tau) f_L}{\mathrm{B}_n}\,(°) \quad (76)$$

where, a is the scale factor, with $a = 144$ for a second-order loop and $a = 160$ for a third-order loop, $\sigma_\mathrm{A}(\tau)$ is the root of Allan variance for the short-term gate time, τ, which is equal to $1/\,\mathrm{B}_n$, and f_L is the L1 frequency.

The PLL dynamic stress error is shown in Tab. IV, where dR is the change of the receiver's position.

From Tab. IV, one can see that PLL dynamic stress error depends on both the loop order and receiver dynamics. In order to decrease the dynamic stress error, the first important task is to determine the level of dynamics and the kind of dynamics the receiver is experiencing, e.g., is the vehicle moving smoothly with high acceleration and small jerk? Or is one dealing with an aircraft wing vibrating with small acceleration and high jerk?

In a digital receiver, there are two other error sources that will increase PLL phase tracking error (Gao (2007, [16])).

The first one is Doppler tracking error Δf, which is usually induced by receiver dynamics. Besides PLL dynamic stress error shown in Table 4, the receiver dynamics will also induce (will cause to appear, or bring about, or produce) Doppler tracking error Δf, and this Doppler error Δf will generate accumulated phase tracking error in every one PIT interval of a digital PLL. This additional PLL phase tracking error $\Delta\phi$ in a digital receiver can be expressed as follows (Gao (2007, [16])):

$$\Delta\phi = 360 \cdot \Delta f \cdot T \quad (77)$$

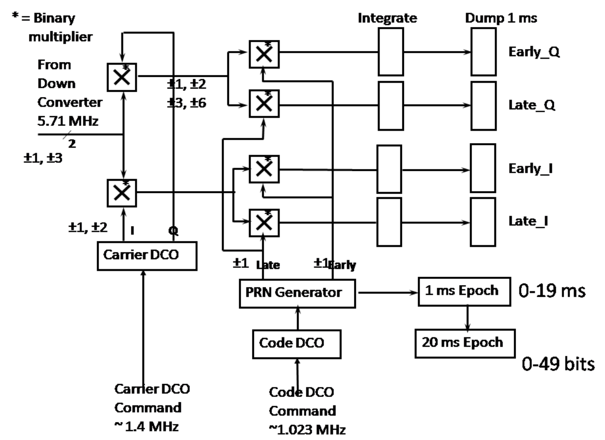

FIGURE 10: GP2021 channel baseband signal processing.

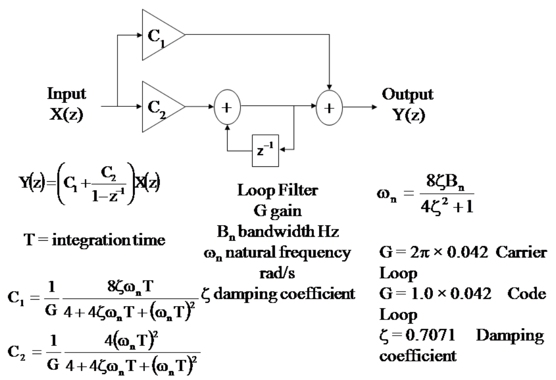

FIGURE 11: Second order tracking loop block diagram in the z domain.

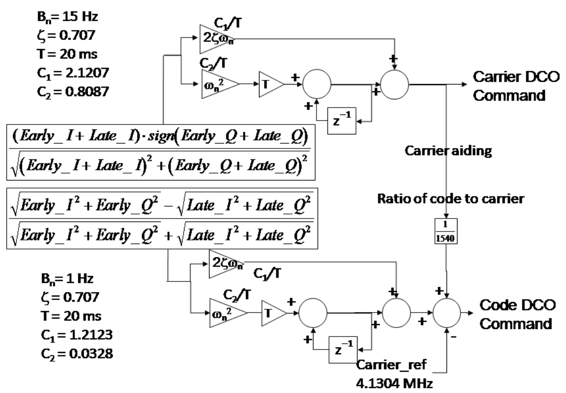

FIGURE 12: GP2021 carrier and code tracking loops.

Similar to the effect of Δf on digital-PLL phase tracking, the instability of receiver oscillator will also increase frequency tracking noise in a PLL and thus generate additional accumulated carrier phase error. This phase tracking error θ_T induced by receiver oscillator (or TCXO) (1 σ) can be expressed as (Gao (2007, [16]))

$$\theta_T = 360 \cdot \sigma_A(\tau) \cdot f_L \cdot T \tag{78}$$

In conclusion, the total PLL tracking error in a digital PLL can be summarized as follows (Gao (2007, [16])):

$$\sigma_{\text{PLL}} = \Delta\phi/3 + \sqrt{\sigma_{PLL,t}^2 + \theta_T^2} + \theta_e/3\ (°) \tag{79}$$

where, Δf is the Doppler error, $\sigma_{\text{PLL,t}}$ is the PLL thermal noise, θ_A is Allan deviation oscillator (or TCXO) phase noise and θ_C is PLL dynamic stress error.

Comparing (79) with (74) for continuous PLL tracking phase error (e.g., Kaplan, Hegarty (1996, [10])), it is clear that the PLL tracking error in a digital FLL is larger than the theoretical error in a continuous system.

Similarly, the total FLL tracking error in a digital FLL can be written as follows (Gao (2007, [16])):

$$\sigma_{\text{FLL}} = \left(\Delta f/3 + \sqrt{\sigma_{FLL,t}^2 + \sigma_A^2 f_L^2} + f_e/3\right) \cdot T\ (\text{Hz}) \tag{80}$$

In order to study the effect of different error sources in a digital PLL, Tab. V, which is based on (75) to (78), gives the PLL phase tracking errors for seven different parameter combinations. In Tab. V, the Doppler error $\Delta f = 0.5$ Hz, the Carrier-to-noise ratio $\mathrm{C/N_0} = 15$ dB-Hz and the root of Allan Variance $\sigma_A = 10^{-10}$are used.

In this table, the first three combinations use the same $\mathrm{C/N_0}$ and PIT. The difference is that different noise bandwidths are adopted to study the effect of noise bandwidth on the PLL phase tracking errors. In Combinations four, five and six, the PIT is tested for the same purpose. From the results of Combinations one to three, it is clear that the most efficient approach to decrease the PLL thermal noise is to decrease the noise bandwidth. The choice of noise bandwidth however, is restricted by receiver dynamics uncertainty and Allan deviation oscillator phase noise. Therefore, the noise bandwidth cannot be decreased endlessly. Increasing PIT, as shown in combinations four to six, also can decrease the thermal noise error. Unfortunately, since digital tracking loops are normally used in a receiver, when the PIT is increased, accumulated phase tracking errors induced by the receiver dynamics uncertainty and the oscillator instability in the integration time increase and lead to an unacceptably high phase tracking error in total.

Based on the classic theory for GPS receiver design, if the incoming signal is 15 dB-Hz, a reasonable set of parameters for the PLL should be 2 Hz bandwidth and 250 ms integration time, which are shown as combination seven in Tab. V. In this combination, one can see that the product of noise bandwidth and integration time is $B_n T = 0.5$. However, because of Doppler tracking error and oscillator instability, there are other two huge phase tracking errors in a digital PLL in combination seven, therefore, this combination can be totally unstable in real applications, depending on on-board oscillator quality and receiver dynamics.

To a large extent we have good predictions of the continuous tracking loop theory when the product $B_n T \sim 0.1$ or 0.2 as indicated in (34); however, in general the continuous tracking loop theory remains silent for value of $B_n T \sim 1$ or some arbitrary values.

Therefore, the purpose of the next section is to provide a complete derivation of the tracking loop theory and then deriving a closed form expression of the stability of the tracking loops, which will lead to a closed form expression of the product $B_n T$.

3 GP2021 Tracking Loops Theory and Practice

The purpose of this section is to introduce the GP2021 tracking loop use in current software implementation by OpenSource GPS Software receiver which was used for our experimental set up.

This section consists of three subsections. First, we discuss the GP2021 channel baseband signal processing. Second, we analyze the GP20201 discrete-time carrier and code tracking loop theory and practice where we derive the discrete-time stability equation for both the carrier and code tracking loops. Third, we discuss the GP2021 carrier tracking loops which is current software implementation by OpenSource GPS Software receiver which was used for our experimental set up.

3.1 GP2021 channel baseband signal processing

Figure 10 illustrates the GPS2021 channel baseband signal processing. The signal coming from the down-converter is multiplied first with the I and Q samples of the carrier digitally controlled oscillator (DCO). The resolution of the DCO is set by the sample frequency divided by the number of possible binary settings. While this is adjustable for a software receiver by emulating the GP2021 this value is set by the manufacturer as 5.714 MHz/2^27bits or 0.042574746 Hz. The Carrier DCO outputs the phase of the IF signal. The highest 3 bits of the DCO register are used to address the sine and cosine tables. The code DCO does the same and generates the phase of the PRN code.

These two signals are binary multiplied by the early and late I and Q PRN samples coming from the PRN generator. The four channels are integrated and dumped to yield the desired signals to compute the time and phase information for the Carrier and Code DCO. Moreover, as seen in Fig. 10 the PRN generator outputs the 1 ms epoch of the code transition and also the 20 ms epoch of the data bit transition.

3.2 GP2021 discrete-time carrier and code tracking loop theory and practice

Figure 11 illustrates the second order tracking loops. Let $X(z)$ denote the Z transform of the input sequence $x(n)$ and Z transform to the output sequence $y(n)$ is given by $Y(z)$

$$Y(z) = \left[C_1 + \frac{C_2}{1-z^{-1}} \equiv H(z)\right] X(z) \tag{81}$$

where $H(z)$ is system function and where the filter coefficient C_1 and C_2 are given by

$$C_1 = 8\chi/\mathrm{den}_C \tag{82}$$

$$C_2 = 4(\omega_n T)^2/\mathrm{den}_C \tag{83}$$

$$\mathrm{den}_C = G[(2+\chi)^2 \equiv 4 + 4\chi + \chi^2] \tag{84}$$

$$\chi = \zeta \omega_n T \tag{85}$$

where T is the PIT. The damping coefficient ζ is given by

$$\zeta = \sqrt{2}/2 = 0.7071067811865475244008443621 \tag{86}$$

and the filter loop gain G are determined from

$$G = 1 \times 0.0042 \text{ (Code Tracking)} \tag{87}$$

$$G = 2\pi \times 0.0042 \text{ (Carrier Tracking)} \tag{88}$$

and the natural frequency ω_n is computed from (Misra, Enge (2006, [20]))

$$\omega_n = 8\zeta B_n/(4\zeta^2 + 1) \tag{89}$$

Utilizing the result of a linear system with stationary random inputs we obtain the following expressions for the most important parameters of the system (Gubner (2006, [21]), Proakis, Manolakis (1996, [22])):

1. Output mean value, μ_y

$$\mu_y = \mathrm{H}(e^{j0})\mu_x \tag{90}$$

2. Input-Output crosscorrelation, $r_{xy}(k)$ and output-input crosscorrelation, $r_{yx}(k)$.

$$r_{xy}(k) = h^*(-k) * r_{xx}(k) \tag{91}$$

$$r_{yx}(k) = h(k) * r_{xx}(k) \tag{92}$$

3. Output autocorrelation, $r_{yy}(k)$

$$r_{yy}(k) = h(k) * r_{xy}(k) \equiv h(k) * h^{*}(-k) * r_{xx}(k) \quad (93)$$

where the symbol (*) is used to denote the time convolution between two waveforms or signals (see (Gubner (2006, [21]), Proakis, Manolakis (1996, [22])).

In all of the above calculations, the system function $H(z)$ plays a major role which is the reason why we need to take a careful look at the nature of the system function, $H(z)$.

Clearly, H(z) has a pole for $z = 1$, which explains why the system will be unstable for $z = 1$. It is important to determine the Region of Convergence (ROC) for this system; i.e., ROC implies the values of z for which the system will be stable and that solution is intrinsically connected with the values of coefficients C_1 and C_2 and with the values of B_nT.

Taking the inverse $\mathcal{Z}$ transform we find the unit impulse response or $h(n)$ given by

$$h(n) = C_1\delta(n) + C_2u(n) \quad (94)$$

where $\delta(n)$ is the Dirac delta function and $u(n)$ is the unit step function.

The condition for stability (or ROC of the unit impose response $h(n)$) can be found from seeking all the value of z for which the absolute value of the system transfer z function $H(z)$ is less than infinity or (Proakis, Manolakis (1996, [22]))

$$|H(z)| = \left|\sum_{n=0}^{\infty} h(n)z^{-n}\right| \leq \sum_{n=0}^{\infty}|h(n)z^{-n}| \leq \sum_{n=0}^{\infty}|h(n)| < \infty \quad (95)$$

Hence, the ROC or the stability of unit impulse response $h(n)$ occurs if and only if (iff)

$$|C_2| < 1 \Leftrightarrow 0 < C_2 < 1 \quad (96)$$

Since the C_2 is positive in (96) is equivalent with

$$0 < C_2 = 4(\omega_nT)^2/\mathrm{den}_C = \alpha_2(B_nT)^2 < 1 \quad (97)$$

$$\alpha_2 = 4 \times [8\zeta/(4\zeta^2 + 1)]^2/\mathrm{den}_C \quad (98)$$

From the left side of the inequality (97) we get

$$B_nT > 0 \quad (99)$$

From the right side of inequality (97) we obtain

$$B_nT < 1/\left[\sqrt{\alpha_2} \equiv 2 \times 8\zeta/(4\zeta^2 + 1)/\sqrt{\mathrm{den}_C}\right] \quad (100)$$

In Appendix A, Dr. Progri have provided the necessary details of the stability for the condition of ω_nT which is the following inequality

$$-\frac{2\sqrt{G}(2-\sqrt{G}\zeta)}{4-G\zeta^2} < 0 < \omega_nT < \frac{2\sqrt{G}(2+\sqrt{G}\zeta)}{4-G\zeta^2} \text{ vii} \quad (101)$$

Since the lower bound is smaller than zero[viii] then we obtain the revised, final inequality for stability condition in terms of ω_nT as follows

$$2\sqrt{G}/(2 + \sqrt{G}\zeta) < \omega_nT < 2\sqrt{G}/(2 - \sqrt{G}\zeta) \quad (102)$$

Now in terms of B_nT by substituting (89) into (102) we get

$$-\frac{(4\zeta^2+1)\sqrt{G}}{8\zeta+4\zeta^2\sqrt{G}} < 0 < B_nT < \frac{(4\zeta^2+1)\sqrt{G}}{8\zeta-4\zeta^2\sqrt{G}} \quad (103)$$

Substituting the numerical values of GP2021 for the damping coefficient ζ (86) yield the following range of values for the stability condition in terms of ω_nT and B_nT

$$0 < \omega_nT < 4\sqrt{G}/(4 - \sqrt{2G}) \quad (104)$$

$$0 < B_nT < 3\sqrt{2G}/(8 - 2\sqrt{2G}) \quad (105)$$

and the gain G (87) and (88) ditto

$0 < \omega_nT < 0.2209$[ix] (code tracking) (106)

$0 < B_nT < 0.1172$[x] (code tracking) (107)

$0 < \omega_nT < 0.6277$[xi] (carrier tracking) (108)

$0 < B_nT < 0.3329$[xii] (carrier tracking) (109)

According to (106) the code tracking will be stable as long as $0 < \omega_nT < 0.2209$ and $0 < B_nT < 0.1172$ and the carrier tracking will be stable as long as $0 < \omega_nT < 0.6277$ and $0 < B_nT < 0.3329$.

For values of $B_nT > 0.1172$ the code tracking will be unstable and for values of $B_nT > 0.3329$ the carrier tracking will be unstable. We remind the reader that the values of B_n for code tracking loop are different from the values of B_n for carrier tracking which is the purpose of Progri et al. (2023, [23]) to consider some applications of the GP20201 discrete-time code and carrier tracking loop implementations.

In conclusion, as illustrated by the theory developed in this section, when B_nT is close to one, signal tracking loops in a digital receiver will become unstable. Furthermore, even when B_nT is much smaller than one, if the integration time T is very long, it is still possible that a digital receiver will crash in run, because the accumulated phase tracking errors induced (caused or produced) by receiver dynamics and oscillator (or TCXO) instability in one integration time interval may reach the tracking threshold.

3.3 GP2021 discrete-time carrier and code tracking loop implementation

Figure 12 shows GP2021 discrete-time carrier and code tracking loops which appear to indicate that for a particular implementation the values of $B_nT = 0.02$ for code tracking and $B_nT = 0.3$ for the carrier tracking. For this particular implementation both the code and carrier tracking are stable. For this particular case $C_1 = 2.12$ and $C_2 = 0.81$ for carrier tracking and $C_1 = 1.21$ and $C_2 = 0.03$ for code tracking. We also have to note that the input signal to the carrier tracking loop filter is different from the input signal to the code tracking loop filter.

This concludes the part one of the paper. In Progri et al. (2023, [23]) we discuss the implementation and testing of the theory presented in this paper.

4 Conclusions

We have presented the discrete vs. continuous tracking loop theory and applications with large B_nT to a great deal of detail. This was made possible by:

1. First, showing a derivation of the continuous (or classic) tracking loop theory and applications on large B_nT. Even for continuous carrier loop or the classic case we did not find an explicit expression of the B_nT.
2. Second, we considered the discrete time tracking loop and we investigated the GP2021 implementation. For this case we were able to come up with an explicit expression of the stability of the discrete-time tracking loop which led to finding the desired region of convergence for $0 < B_nT < 0.3329$; i.e., for values of B_nT inside the region of convergence the carrier tracking will be stable and it will result in a stable output, which is the carrier DCO. On the other hand, for values of B_nT outside the region of convergence the carrier tracking will be unstable which will result in an unstable output.

When B_nT is close to one, signal tracking loops in a digital receiver will become unstable (as proved by Ilir). Furthermore, even when B_nT is much smaller than one, if the integration time T is very long, it is still possible that a digital receiver will crash in run, because the accumulated phase tracking errors induced by receiver dynamics and oscillator instability in one integration time interval may reach the tracking threshold (as proved by Gao). In conclusion, for a digital GPS receiver, the expression for PLL/FLL tracking errors has to be modified. Our paper has shown two new expressions (i.e., (106) through (109)) to calculate the total carrier/carrier phase tracking error in a digital receiver. Furthermore, because signal tracking loops will be unstable, when B_nT is above 0.3329 (for PLL) or 0.1172 (for DLL), therefore, there is a condition which must be added in (106) through (109) and this condition is that $0 < B_nT < 0.3329$ (for PLL, Progri (109)).

5 Future Work

Thus far we were able to come up with a very important condition on the stability of the second order carrier and code tracking loop filters namely (106) through (109).

However, (106) through (109) provides an infinite number of combinations of the product B_nT and further more results with real data appear to indicate that for very small values of T there is a large variance associated with the phase noise.

We believe that the direction towards which this investigation should is to come up with a closed form analytical expression that will provide the minimum accumulated carrier phase variance as a function of the B_nT. The results of our future investigation will be published as a follow up paper in one of the future proceedings of the Institute of Navigation and in the Giftet Journal of Geolocation, Geo-information, and Geo-intelligence.

6 Acknowledgement

The publication of this work in the Giftet Journal of Geolocation, Geoinformation, and Geo-intelligence was supported by Giftet Inc. executive office.

The authors would like to thank The Open-Source GPS, The University of Calgary, Point Inc, WPI, The University of New South Wales, The Advanced Research Corp., and The Institute of Navigation for their continued support. The author would also like to thank the session chair and the program committee for accepting our paper at the ION GNSS 2007.

7 References

[1] I. Progri, C.W. Kelley, G. Gao, W.R. Michalson, J. Wang, J. Lavrakas, "Discrete vs. continuous carrier tracking loop theory, implementation, and testing with large BnT," in *Proc. 20th Intr. Tech. Mtg. Sat. Div. ION (ION GNSS 2007)*, Fort Worth, TX, pp. 2584-2610, Sep. 2007, http://giftet.com/Progri/Progri_2007_09_02_ION_GNSS.pdf.

[2] J.J. Spilker Jr., "Fundamentals of signal tracking theory," Chap. 7 of *Global Positioning System: Theory and Applications*. Vol. I. (Edited by B.W. Parkinson, J.J. Spilker Jr & Associate Editors P. Axelrad, P. Enge), Washington, DC: AIAA, pp 121-176, 1996.

[3] M. Zhodzishsky, S. Yudanov, V. Veitsel, J. Ashjaee, "Co-OP tracking for carrier phase," in *Proc. of the 11th Intern. Tech. Mtg. of the Sat. Div. of ION (ION GPS 1998)*, Nashville, TN, pp. 653-664, Sep. 1998.

[4] D. Gustafson, J. Dowdle, K. Flueckiger, "A high anti-jam GPS based navigator," in *Proc. ION Nat. Tech. Mtg. (NTM),* 26-28 January, Anaheim CA, pp. 495-503, ION, Fairfax VA, 2000.

[5] M.L. Psiaki, H. Jung, "Extended Kalman filter methods for tracking weak GPS signals," in *Proc. of ION GNSS*, Portland, OR, pp. 2539-2553, Sep. 2002.

[6] I. Progri, "An assessment of indoor geolocation systems," *Ph.D. Dissertation*, Worcester Polytechnic Institute, 408 pg., May 2003, URL: http://giftet.com/Progri/Progri_2003_05_Ph.D._Dissertation.pdf.

[7] I. Progri, W.R. Michalson, J. Wang, M.C. Bromberg, "Indoor geolocation using FCDMA pseudolites: signal structure and performance analysis," *Navigation*, vol. 54, no. 3, pp. 242-256, fall 2007, DOI: http://dx.doi.org/10.1002/j.2161-4296.2007.tb00407.x, http://giftet.com/Progri/Progri_2007_fall_Navigation.pdf.

[8] I. Progri, P. Huang, Y. Pi, X. Xia, "Indoor adaptive GNSS signal acquisition. Part 1: theory and simulations," *J. Geol. Geoinfo. Geointel.,* vol. 2016, article ID 2016071601, 19 pg., Nov. 2016. DOI: http://doi.org/10.18610/JG3.2016.071601, http://giftet.com/JG3/2016/071601.pdf.

[9] I.F. Progri, W.R. Michalson, "An underground system of stationary pseudolites," *J. Geol. Geoinfo. Geointel.*, vol. 2020, article ID 2020071605, 10 pg., Nov. 2020. DOI: http://doi.org/10.18610/JG3.2020.071605, http://giftet.com/JG3/2020/071605.pdf.

[10] E.D. Kaplan, C. Hegarty. *Understanding GPS: Principles and Applications 2nd ed.*, Boston MA: Artech House, 1996.

[11] O. Julien, "Design of Galileo L1F Receiver Tracking Loops", *Ph.D. Dissertation*, published as Report No. 20227, Department of Geomatics Engineering, The University of Calgary, Canada, 2005 (Available at http://plan.geomatics.ucalgary.ca).

[12] O. Julien, "Carrier-phase tracking of future data/pilot signals," in *Proc. 18th Inter. Tech. Mtg. Sat. Div. ION (ION GNSS 2005)*, Long Beach, CA, pp. 113-124., Sep. 2005.

[13] I. Progri, *Geolocation of RF Signals—Principles and Simulations*. 1st ed., New York, NY: Springer Science & Business Media, LLC, 330 pg., Jan. 2011, DOI: http://doi.org/10.1007/978-1-4419-7952-0, URL: http://springer.com/engineering/electronics/book/978-1-4419-7951-3.

[14] I.F. Progri, "The evolution of the (terrestrial) navigator," in Proc. ION-GNSS+ 2022, Denver, CO, pp. 1809-1830, Sep. 2022, https://doi.org/10.33012/2022.18505, http://giftet.com/Progri/Progri_2022_09_01_ION_GNSS+.pdf.

[15] S.A. Stephens, J.B. Thomas, "Controlled-root formulation for digital phase-locked loops," *IEEE Trans. on Aero. Elec. Sys.,* vol. 31, no. 1, pp. 78-95, 1995, DOI: https://doi.org/10.1109/7.366295.

[16] G. Gao, "INS-assisted high sensitivity GPS receivers for degraded signal navigation," *Ph.D. Dissertation*, (Published as Reports Number 20252), Department of Geomatics Engineering, University of Calgary, Canada, Feb. 2007. (Available at http:\plan.geomatics.ucalgary.ca).

[17] J.F. Raquet, GPS receiver design, *ENGO 699.10 Course Notes*, Department of Geomatics Engineering, University of Calgary, Canada, 2004.

[18] R. Watson "High-sensitivity GPS L1 signal analysis for indoor channel modelling". *MS Thesis*, (published as Report No. 20215,) Department of Geomatics Engineering, The University of Calgary, Canada, 2005 (Available at http://plan.geomatics.ucalgary.ca)

[19] C. Ma, G. Lachapelle, M.E. Cannon, "Implementation of a software GPS receiver," *in Proc; of ION GNSS*, Long Beach CA, pp. 956-970, Sep. 2004.

[20] P. Misra, P. Enge, *Global Positioning System–Signals Measurements and Performance 2nd ed.*, Lincoln, MA: Ganga-Jamuna Press, 2006.

[21] J.A. Gubner, *Probability and Random Processes for Electrical and Computer Engineers*. Cambridge, UK: Cambridge Univ. Press, 2006.

[22] J.G. Proakis, D.G. Manolakis, *Digital Signal Processing: Principles, Algorithms, and Applications*, Upper Saddle River, NJ: Prentice-Hall, 1996.

[23] I. Progri, C.W. Kelley, G. Gao, W.R. Michalson, J. Wang, J. Lavrakas, "Discrete vs. continuous carrier tracking loop with large BnT: part 2, implementation and testing," *J. Geol. Geoinfo. Geointel.,* vol. 2023, article ID 2023071602, 13 pg., Nov. 2023. DOI:

http://doi.org/10.18610/JG3.2023.071602, http://giftet.com/JG3/2023/071602.pdf.

[24] I. Progri, *Indoor Geolocation Systems—Theory and Applications*. *I*, 1st ed., Worcester, MA: Giftet Inc., ~800 pp., ~ 2024 (not yet available in print).

[25] Anon. "Crystal oscillator," From Wikipedia, the free encyclopedia June 2023, https://en.wikipedia.org/wiki/Crystal_oscillator.

8 Appendix A: Derivation of the revised inequality of B_nT

In Appendix A, I provide the details for the derivation of the inequality of B_nT. Recall from (100) we have the following inequality:

$$B_nT < 1/\left[\sqrt{\alpha_2} \equiv 2 \times 8\zeta/(4\zeta^2+1)/\sqrt{\mathrm{den}_C}\right]$$
$$= \sqrt{\mathrm{den}_C}/[16\zeta/(4\zeta^2+1)]$$
$$= (4\zeta^2+1)\sqrt{G(2+\chi)^2}/16\zeta$$
$$= (4\zeta^2+1)\sqrt{G}(2+\chi)/16\zeta$$
$$= (4\zeta^2+1)\sqrt{G}/8\zeta + (4\zeta^2+1)\sqrt{G}\chi/16\zeta$$
$$= (4\zeta^2+1)\sqrt{G}/8\zeta + (4\zeta^2+1)\sqrt{G}\omega_nT/16$$
$$= (4\zeta^2+1)\sqrt{G}/8\zeta + \sqrt{G}\zeta B_nT/2 \quad (110)$$

Taking the B_nT on the lefthand side we obtain

$$B_nT\left(1-\sqrt{G}\zeta/2\right) < (4\zeta^2+1)\sqrt{G}/8\zeta \quad (111)$$

which provides the desired inequality of the B_nT as follows

$$B_nT < (4\zeta^2+1)\sqrt{G}/8\zeta/\left(1-\sqrt{G}\zeta/2\right)$$
$$= (4\zeta^2+1)\sqrt{G}/\left(8\zeta - 4\zeta^2\sqrt{G}\right) \quad (112)$$

Substituting the values of damping coefficient ζ from (86) yields

$$B_nT < 3\sqrt{G}/\left(4\sqrt{2}-2\sqrt{G}\right) = 3\sqrt{2G}/\left(8-2\sqrt{2G}\right) \quad (113)$$

A slightly different approach is given below. First, we want the following inequality

$$C_2 = 4(\omega_nT)^2/\mathrm{den}_C < 1 \quad (114)$$
$$4(\omega_nT)^2 < G(2+\chi)^2 \quad (115)$$

which is equivalent with

$$2\omega_nT < \sqrt{G}(2+\zeta\omega_nT) \quad (116)$$

Taking the ω_nT on the lefthand side we obtain

$$\left(2-\sqrt{G}\zeta\right)\omega_nT < 2\sqrt{G} \quad (117)$$

Substituting (89) for ω_n into (117) on the lefthand side produces

$$B_nT\left(2-\sqrt{G}\zeta\right)8\zeta/(4\zeta^2+1) < 2\sqrt{G} \quad (118)$$

After some elementary algebra the above is reduced to

$$B_nT4\zeta\left(2-\sqrt{G}\zeta\right) < (4\zeta^2+1)\sqrt{G} \quad (119)$$

Which leads to the final solution of the desired inequality of B_nT as follows

$$B_nT < (4\zeta^2+1)\sqrt{G}/\left(8\zeta-4\zeta^2\sqrt{G}\right) \quad (120)$$

There is no surprise that (120) is exactly the same as (112). The only one problem with the first two approaches is that they eliminate one of the bounds by taking the square root of the solution. This problem can be fixed by looking at the solution of the quadratic equation which was initially discussed in Progri et al (2007, [1]).

Next, let us rederive the solution for the inequality of the B_nT based on the derivations in Progri et al (2007, [1]).

$$4(\omega_nT)^2 < G[4+4\zeta\omega_nT+(\zeta\omega_nT)^2]$$
$$= 4G + 4G\zeta\omega_nT + G\zeta^2(\omega_nT)^2 \quad (121)$$

Re-arranging the terms in (121) we obtain the following

$$(G\zeta^2-4)(\omega_nT)^2 + 4G\zeta\omega_nT + 4G > 0^{\mathrm{xiii}} \quad (122)$$
$$16G^2\zeta^2 - 16G(G\zeta^2-4) = 4\times 16G \quad (123)$$

Substituting (123) into Progri et al (2007, [1])

$$\omega_nT > \left(-4G\zeta+\sqrt{4\times16G}\right)/[2(G\zeta^2-4)]$$
$$= 2\sqrt{G}\left(2-\sqrt{G}\zeta\right)/(G\zeta^2-4)$$
$$= -2\sqrt{G}\left(2-\sqrt{G}\zeta\right)/(4-G\zeta^2)$$
$$= -2\sqrt{G}/\left(2+\sqrt{G}\zeta\right) \quad (124)$$
$$\omega_nT < \left(-4G\zeta-\sqrt{4\times16G}\right)/[2(G\zeta^2-4)]$$
$$= 2\sqrt{G}\left(2+\sqrt{G}\zeta\right)/(4-G\zeta^2)$$
$$= 2\sqrt{G}/\left(2-\sqrt{G}\zeta\right) \quad (125)$$

Combining these two solutions together produces:

$$-2\sqrt{G}/\left(2+\sqrt{G}\zeta\right) < 0 < \omega_nT < 2\sqrt{G}/\left(2-\sqrt{G}\zeta\right) \quad (126)$$

Substituting (89) into Progri et al (2007, [1]) (121) produces,

$$-\frac{(4\zeta^2+1)\sqrt{G}}{8\zeta+4\zeta^2\sqrt{G}} < 0 < B_nT < \frac{(4\zeta^2+1)\sqrt{G}}{8\zeta-4\zeta^2\sqrt{G}} \quad (127)$$

The righthand side of inequality (127) is exactly the same as the solution in (120) and (112). However, I have added an original inequality on the righthand side of (127); therefore, both sides of inequality (127) provide more insights than the initial inequality in Progri et al (2007, [1]) (46) and (47).

Substituting the values of damping coefficient ζ from (86) into (127) yields

$$-\frac{4\sqrt{G}}{4+\sqrt{2G}} < 0 < \omega_nT < \frac{4\sqrt{G}}{4-\sqrt{G2}} \quad (128)$$

$$-\frac{3\sqrt{2G}}{8+2\sqrt{2G}} < 0 < B_nT < \frac{3\sqrt{2G}}{8-2\sqrt{2G}} \quad (129)$$

The new range of stability for both ω_nT and B_nT is narrower than what was initially proposed from Progri et al (2007, [1]) (46) and (47); which means that (127) provides significantly improved bounds.

Moreover, the righthand side of (127) is identical to both (120) and (112).

---

[i] This article was originally published in Progri et al., (2007, [1]). This is a significantly improved revision of the same ION GNSS 2007 conference paper. This journal paper includes a major revision of the equations, addition of the Appendix A, and refinement of the bounds of the $\omega_n T$ and $B_n T$.

[ii] See (11).

[iii] See (12)

[iv] See (11).

[v] See (12).

[vi] Temperature influences the operating frequency; various forms of compensation are used, from analog compensation (TCXO) and microcontroller compensation (MCXO) to stabilization of the temperature with a crystal oven (OCXO). The crystals possess temperature hysteresis; the frequency at a given temperature achieved by increasing the temperature is not equal to the frequency on the same temperature achieved by decreasing the temperature. The temperature sensitivity depends primarily on the cut; the temperature compensated cuts are chosen as to minimize frequency/temperature dependence. Special cuts can be made with linear temperature characteristics; the LC cut is used in quartz thermometers. Other influencing factors are the overtone used, the mounting and electrodes, impurities in the crystal, mechanical strain, crystal geometry, rate of temperature change, thermal history (due to hysteresis), ionizing radiation, and drive level [25].

[vii] There is an error in Progri et al. (2007, [1]) (45); the term ζ^2 is missing. It is corrected in (101).

[viii] Not less than zero as mistakenly reported in Progri et al (2007, [1]).

[ix] This is corrected from 0.2216 that was initially reported in Progri et al (2007, [1]).

[x] Ditto 0.16.

[xi] Ditto 0.6407.

[xii] Ditto 0.34.

[xiii] There is an error in Progri et al (2007, [1]) (44); the term ζ^2 is missing. It is corrected in (122).